JOURNAL OF CATALYSIS 31, 41–50 (1973)

The Non-Isothermal Catalytic Effectiveness Factor for Monolith Supported Catalysts

J. J. CARBERRY AND A. A. KULKARNI

Department of Chemical Engineering, University of Notre Dame, Notre Dame, Indiana 46556

Received March 12, 1973

Catalytic effectiveness factor relationships expressed in terms of laboratory observables are derived for monolith supported catalysts in instances in which (a) a nonporous monolith sustains an n^{th} order ($n \gtreqless 1$) reaction in the presence of external temperature and concentration gradients, and (b) an isothermal diffusion affected porous monolith sustains first order reaction in the presence of external temperature and concentration gradients. Further, a simple relationship is presented which testifies to the validity of the isothermal pellet assumption, hence the derived effectiveness for the porous monolith is applicable to muffler systems composed of pelleted catalysts. Finally, for the case of negative order kinetics, as found in CO oxidation over Pt, Pd, Rh and Ru, multiple steady states and regimes of instability are cited which combined with the rate-enhancing effects of axial dispersion, tend to clarify the noted thermal instability of noble metal catalyst systems.

INTRODUCTION

The requirement that an automotive emissions abatement catalytic system exhibit rapid warm-up characteristics and durability has prompted the development of a novel support system—the monolith, consisting in general of an often parallel network of thin-walled channels. A thin layer of catalyst support (usually alumina) coats the monolith channel walls and the active catalyst is deposited thereupon. Variations upon the parallel thin-wall channel design exist: complex honeycombs of interconnecting thin-wall channels, etc. Whatever the variation, all monoliths are characterized by a very thin layer of supported catalyst deposited upon a thin monolith subsupport.

Given the rapidity and exothermicity of the emissions combustion reactions, one may justly anticipate heat and mass diffusional intrusions. In fact, such intrusions should be encouraged since the survival of partially oxidized intermediates is to be avoided (*1–3*). However, means whereby an assessment of diffusional influences may be realized seem not to be on hand, as the monolith system departs from the pellet/extrusion formulations upon which diffusion–catalytic reaction analyses have been traditionally established (*4–6*).

PHYSICAL MODELS

We consider two models of catalysis upon monoliths:

(a) As set forth in Fig. 1a, the catalytic agent is assumed to exist upon a nonporous monolith supported substrate (e.g., a very thin layer of alumina). A surface reaction of n^{th} order occurs and under diffusional retardation, surface temperature and concentration do not equal bulk values within the monolith channel. ($C_s < C_o$; $T_o < T_s$). For exothermic reactions $T_o < T_s$; for endothermic cases $T_o > T_s$.

(b) As shown in Fig. 1b, the monolith structure is assumed to support a finite isothermal layer of porous support within

which the catalyst is impregnated. Thus, gradients can, in principle, exist within the porous structure, as well as in the boundary layers, as in case (a). Only linear kinetics are considered in this case (b). ($C < C_s < C_o$; $T_o < T_s = T$). Clearly case (b) reduces to case (a) when the zone of intraphase reaction retreats to the external surface of the porous support layer.

We seek simple analytical relationships between the catalytic effectiveness and the observable parameters for each monolith system.

Theory

Case (a): Nonporous Monolith

Catalytic effectiveness for n^{th} order reaction is defined as

$$\bar{\eta} = k_s C_s^n / k_o C_o^n = \frac{\text{rate at } T_s \text{ and } C_s}{\text{rate at } T_o \text{ and } C_o} \quad (1)$$

Equating the rate of external mass transport to that of surface reaction

$$k_g a(C_o - C_s) = k_s C_s^n,$$

we obtain

$$C_s/C_o = 1 - \frac{k_s C_o^{n-1}}{k_g a}\left(\frac{C_s}{C_o}\right)^n \quad (2)$$

Now in view of Eq. (1), the observed rate $\mathcal{R}_o$ is

$$\mathcal{R}_o = \bar{\eta} k_o C_o^n = k_s C_s^n$$

Dividing by $k_g a C_o$,

$$\mathcal{R}_o/k_g a C_o = \bar{\eta}(k_o C_o^{n-1}/k_g a) = (k_s C_o^{n-1}/k_g a)(C_s/C_o)^n. \quad (3)$$

We define the Damköhler number, Da_o

$$Da_o = k_o C_o^{n-1}/k_g a.$$

Hence

$$\mathcal{R}_o/k_f a C_o = \bar{\eta} Da_o = (k_s C_o^{n-1}/k_g a)(C_s/C_o)^n = \text{observable parameter} \quad (4)$$

By Eqs. (2) and (4)

$$C_s/C_o = 1 - \bar{\eta} Da_o$$

and thus by Eq. (1)

$$\bar{\eta} = (k_s/k_o)(1 - \bar{\eta} Da_o)^n. \quad (5)$$

Further

$$\frac{k_s}{k_o} = \exp\left[-\frac{E}{R}\left(\frac{1}{T_s} - \frac{1}{T_o}\right)\right] = \exp\left[-\epsilon_o\left(\frac{1}{t} - 1\right)\right], \quad (6)$$

where $\epsilon_o = E/RT_o$ and $t = T_s/T_o$.

Equation 6 assumes that the Arrhenius pre-exponential factor is temperature independent, a reasonable assumption, indeed.

We have now to establish t in terms of the observable $\bar{\eta} Da_o$. A heat balance relating heat generation at the monolith surface to convective transfer yields

$$ha(T_s - T_o) = (-\Delta H)\mathcal{R}_o. \quad (7)$$

Dividing by $k_g a C_o T_o$,

$$(h/k_g a C_o)(t - 1) = (-\Delta H/T_o)(\mathcal{R}_o/k_g a C_o) = (-\Delta H/T_o)\bar{\eta} Da_o \quad (8)$$

The convective coefficients h and k_g are related by the well-known heat–mass transport analogy (7)

$$j_D = j_H$$

or

$$(k_g/u)(Sc)^{2/3} = (h/\rho C_p u)(Pr)^{2/3},$$

where u is fluid velocity, ρC_p the volumetric heat capacity of the fluid, and

Sc = Schmidt number $= \dfrac{\text{kinematic viscosity}}{\text{molecular diffusivity}}$

Pr = Prandtl number $= \dfrac{\text{kinematic viscosity}}{\text{thermal diffusivity}}$.

Therefore,

$$h/k_g = \rho C_p (Sc/Pr)^{2/3} = \rho C_p (Le)^{2/3}, \quad (9)$$

where Le = Lewis number $= \dfrac{\text{thermal diffusivity}}{\text{molecular diffusivity}}$ of the fluid.

The surface temperature t in terms of the observable and thermal characteristic of the system is, then, by Eqs. (8) and (9)

$$t = 1 + [(-\Delta H)C_o/\rho C_p T_o]\frac{1}{Le^{2/3}}\bar{\eta} Da_o$$

or $$t = 1 + \bar{\beta}\bar{\eta} Da_o. \quad (10)$$

In consequence, the local non-isothermal catalytic effectiveness for the nonporous monolith catalytic system is solely a function of the observable for given values of ϵ_o and $\bar{\beta}$ and any reaction order, n.

$$\bar{\eta} = (1 - \bar{\eta}Da_o)^n \times \exp\left[-\epsilon_o\left(\frac{1}{1 + \bar{\beta}\bar{\eta}Da_o} - 1\right)\right]. \quad (11)$$

While Eq. (11) is subject to simple manual computation, in Figs. 2 and 3, the $\bar{\eta}$ – observable behavior for diverse reaction orders is set forth for practical values of ϵ_o. Figures 4 and 5 reveal the first order behavior for exothermal and endothermal reaction for diverse values of $\bar{\beta}$ and ϵ_o. By contrast, the isothermal relationships are shown in Fig. 6, where, of course, as Aris noted (*8*) in his reading of Cassiere's work (*9*),

$$\bar{\eta}_{ISO} = (1 - \bar{\eta}Da_o)^n \quad (12)$$

which follows from Eq. (11) at $t = 1$.

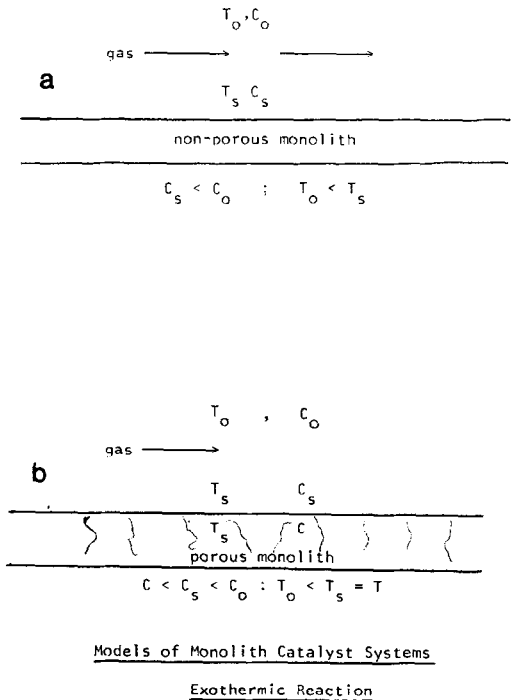

FIG. 1. Model of nonporous (a) and porous (b) monolith catalyst.

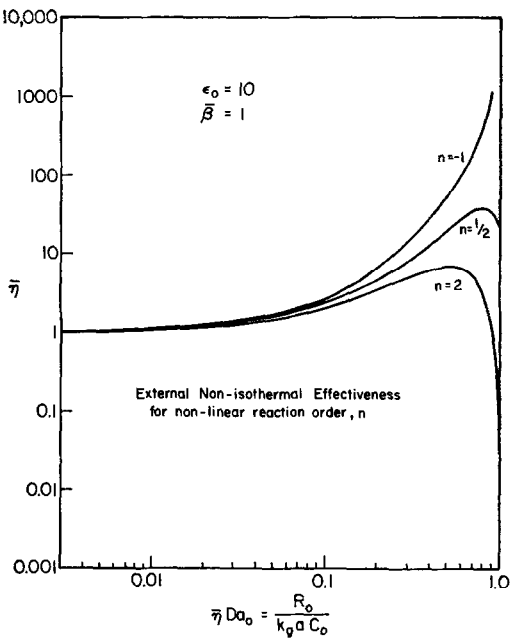

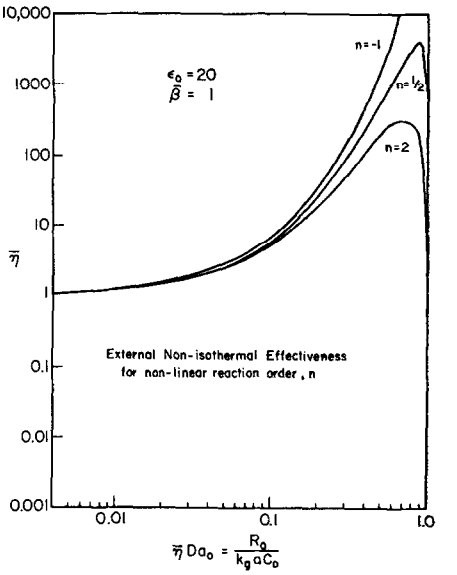

FIGS. 2, 3. External catalytic effectiveness factor for nonlinear kinetics vs observable.

Case (b): Porous Monolith System

Catalytic effectiveness in this non-isothermal instance is, for linear kinetics:

$$\bar{\eta} = \frac{\frac{1}{L}\int_0^L kC\,dz}{k_o C_o}, \quad (13)$$

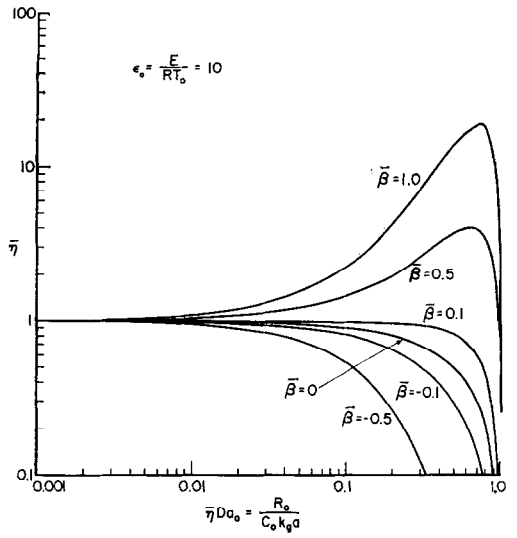

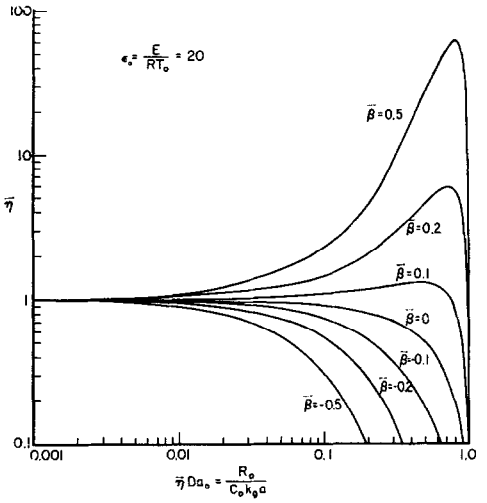

FIGS. 4, 5. External catalytic effectiveness factor for linear kinetics vs observable.

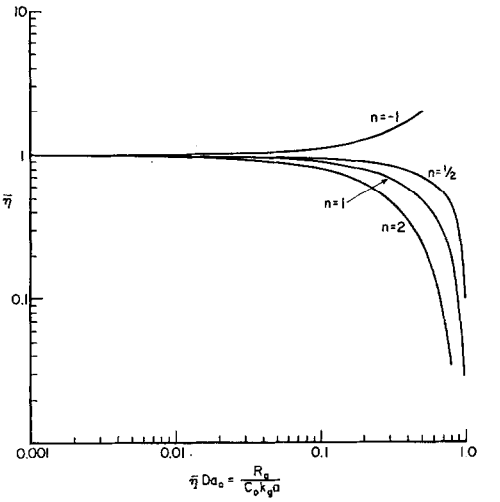

FIG. 6. Isothermal external catalytic effectiveness factor for diverse kinetics vs observable.

where L is the thickness of the porous support deposited on the monolith base. Given the fact that L is indeed small, and earlier teachings (*10,11*) which indicate that in a gas–porous solid catalyst system, the major temperature gradient will be external while the seat of concentration gradients will be within the porous structure, we treat Case (b) as consisting of an isothermal porous medium at a temperature dictated by the external heat transfer resistance. Concentration gradients are anticipated for both the internal and external field. Equation (13) under these conditions becomes

$$\bar{\eta} = \left(\frac{k}{k_o}\right) \frac{\frac{1}{L}\int_0^L C\, dz}{C_o} = \frac{k}{k_o}\eta_t, \qquad (14)$$

where η_t is the isothermal effectiveness evaluated at the catalyst surface temperature, t. The solution, in terms of external mass transport, is (11),

$$\eta_t = \frac{\tanh \phi}{\phi\left[1 + \frac{\phi \tanh \phi}{(Bi)_m}\right]},$$

where $\phi = L\sqrt{\frac{\bar{k}}{\mathfrak{D}}}$, Thiele modulus at temperature t, and $(Bi)_m$ = mass Biot number, $k_g L/\mathfrak{D} = \frac{\text{external}}{\text{internal}}$ transport.

Recalling equation (6), effectiveness for the porous monolith is, therefore,

$$\bar{\eta} = \frac{\tanh \phi}{\phi\left[1 + \frac{\phi \tanh \phi}{(Bi)_m}\right]} \times \exp\left[-\epsilon_o\left(\frac{1}{t} - 1\right)\right]. \qquad (15)$$

As t is given by equation (10) in terms of the observable $\bar{\eta}Da_o$, then Eq. (15) pro-

vides $\bar{\eta}$ as a function of $\bar{\eta}Da_o$, and the Thiele modulus ϕ at the unobserved surface temperature t. We can, however, relate ϕ to $\bar{\eta}Da_o$. The global rate is

$$\mathcal{R}_o = \bar{\eta}k_oC_o.$$

Dividing both sides by $\mathcal{D}C_o/L^2$

$$\frac{L^2\mathcal{R}_o}{C_o\mathcal{D}} = \frac{\phi \tanh \phi}{\left[1 + \dfrac{\phi \tanh \phi}{(Bi)_m}\right]} = \eta\phi^2 \qquad (16)$$

$\dfrac{L^2\mathcal{R}_o}{C_o\mathcal{D}}$ = Weisz number, an observable.

Note, however, that (*11*, *12*)

$$\eta\phi^2/(Bi)_m = \bar{\eta}Da_o \qquad (17)$$

so

$$\bar{\eta}Da_o = \frac{\phi \tanh \phi}{\left[1 + \dfrac{\phi \tanh \phi}{(Bi)_m}\right](Bi)_m} \qquad (18)$$

Equation (15) is simply solved by (I) evaluating $\bar{\eta}Da_o$ by equation (18) for various values of ϕ, and (II) evaluating $\bar{\eta}$ by Eq. (15) for various values of ϕ and corresponding values of $\bar{\eta}Da_o$ as secured by Eq. (18).

There then results an $\bar{\eta}$—observable relationship for specific values of $\bar{\beta}$ and ϵ_o and the mass Biot number, Bi_m. In Figs. 7–10, there are displayed $\bar{\eta}$–$\bar{\eta}Da_o$ relationships for $Bi_m = 10$ and 100 and $\epsilon_o = 10$ and 20, at various values of $\bar{\beta}$.

Validity of Model

It is worth noting that the internal non-isothermal effectiveness factor has been presented (*5*, *6*, *10*) in terms of

$$\beta' = (-\Delta H C_s \mathcal{D}/\lambda T_s) = \text{Prater number.} \qquad (19)$$

The maximum internal temperature relative to the surface value is (13)

$$T_i = T_s(1 + \beta')$$

β' is uniquely related to the external $\bar{\beta}$ used in this external–internal problem by (see Table 1 for definitions of various β's)

$$\beta' = \bar{\beta}(Bi_h/Bi_m)(C_s/C_o)(T_o/T_s). \qquad (20)$$

As has been shown earlier (*10*, *11*), the

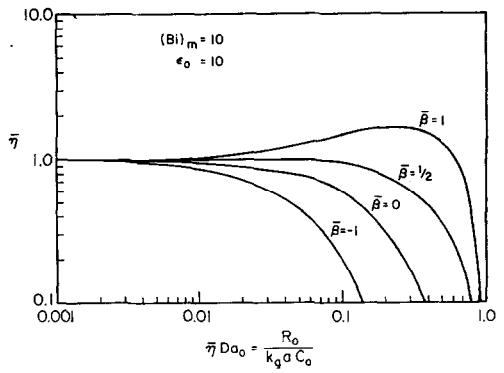

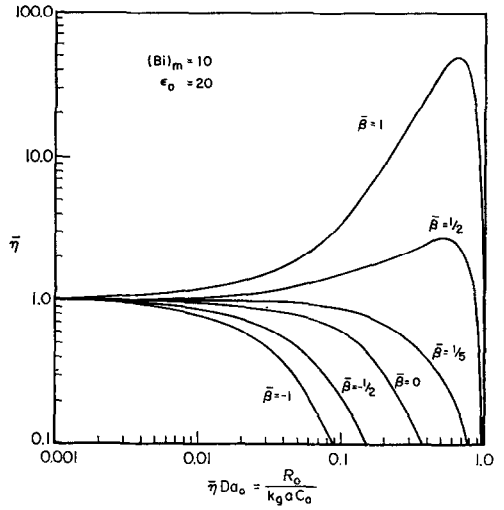

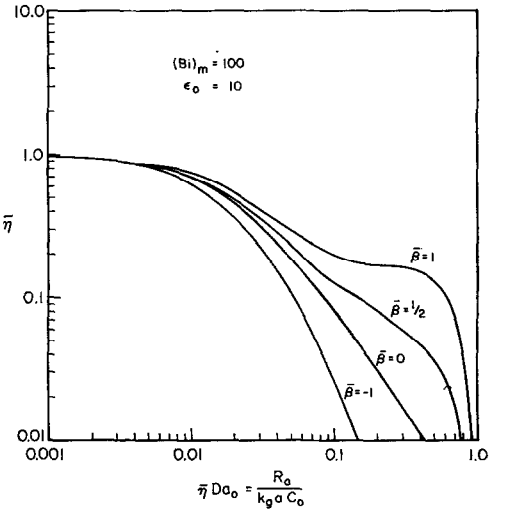

FIGS. 7–10. Internal–external catalytic effectiveness factor vs observable.

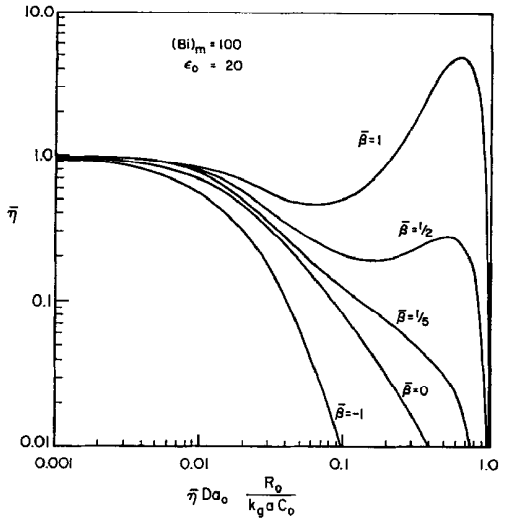

FIG. 10 (*Continued*)

ratio of the thermal $(Bi)_h$ to mass (Bi_m) Biot numbers for gas-solid systems is, where λ is pellet conductivity, ρC_p the volumetric heat capacity of the gas, and $\mathfrak{D}$, intrapellet diffusivity,

$$\rho C_p \mathfrak{D}/\lambda \cdot Le^{2/3} = 10^{-1} \text{ to } 10^{-5}.$$

Hence, $\beta' \ll \bar{\beta}$ by Eq. (20); which teaches, once again, that internal temperature gradients are indeed negligible relative to those existing in the external boundary layers (*14*).

In point of fact, some very sound estimates of the importance of the external temperature gradient relative to that within a porous catalyst can be secured solely in terms of our observable, $\bar{\eta}Da_o$, and the ratio of the Biot numbers.

In the spirit of the development of Lee and Luss (*15*), we proceed as follows: the internal gradient is, relative to surface temperature T_s

$$\Delta T_i/T_s = (-\Delta H)\mathfrak{D}(C_s - C_m)/\lambda T_s.$$

When C_m, the concentration within the pellet center is zero, we have the maximum ΔT_i or

$$(\Delta T_i/T_s)_{\max} = \beta' \tag{21}$$

By Eq. (10) the external ΔT_x, relative to bulk temperature, T_o is

$$\Delta T_x/T_o = \bar{\beta}\bar{\eta}Da_o. \tag{22}$$

Equation (21) contains the unobserved surface concentration C_s, which is readily expressed in terms of observables since

$$k_g a(C_o - C_s) = \eta_i k_s C_s, \tag{23}$$

where η_i is internal effectiveness. But $\eta_i k_s C_s = \mathcal{R}_o$; the observed rate. Hence dividing Eq. (23) by $k_g a C_o$ and solving for C_s, we obtain

$$C_s = C_o(1 - \bar{\eta}Da_o)$$

and by Eq. (21), we obtain

$$\Delta T_i = T_m - T_s = \frac{(-\Delta H)\mathfrak{D}C_o}{\lambda} \cdot (1 - \bar{\eta}Da_o). \tag{24}$$

By Eq. (22), we obtain

$$\Delta T_x = T_s - T_o = [(-\Delta H)C_o/\rho C_p Le^{2/3}] \times \bar{\eta}Da_o \tag{25}$$

Adding Eq. (24) to Eq. (25), we secure the total temperature difference between catalyst centerline T_m and bulk fluid T_o, normalized by T_o

TABLE 1
DEFINITIONS OF BETA VALUES

$$\bar{\beta} = (-\Delta H)C_o/\rho C_p T_o Le^{2/3} = (T_s - T_o)/T_o$$
$$\beta' = (\Delta H)\mathfrak{D}C_s/\lambda T_s = (T_m - T_s)/T_s = \bar{\beta}(Bi_h/Bi_m)(C_s/C_o)(T_o/T_s)$$
$$\beta'_o = (-\Delta H)\mathfrak{D}C_o/\lambda T_o = \beta'(C_o/C_s)(T_s/T_o) = \bar{\beta}(Bi_h/Bi_m)$$
$$\beta_f = (-\Delta H)C_f/\rho C_p T_f = (T_o - T_f)/T_f$$
$$\bar{\beta}_f = (-\Delta H)C_f/\rho C_p T_f Le^{2/3} = \beta_f/Le^{2/3}$$

Subscripts:

- o local bulk fluid value
- s local surface value
- f feedstream value

$$(T_m - T_o)/T_o = \bar{\beta}\bar{\eta}Da_o + \beta'_o(1 - \bar{\eta}Da_o)$$

But since

$$\bar{\beta} = \beta'_o(Bi_m/Bi_h),$$

where $$\beta'_o = (-\Delta H)C_o\mathfrak{D}/\lambda T_o, \qquad (26)$$

then

$$\frac{T_m - T_o}{T_o} = \frac{\Delta T_o}{T_o} = \beta'_o\left[1 + \bar{\eta}Da_o\left(\frac{Bi_m}{Bi_h} - 1\right)\right] \qquad (27)$$

Dividing Eq. (22) by Eq. (27), we obtain the fraction of the total ΔT which resides in the external fluid film,

$$\frac{\Delta T_x}{\Delta T_o} = \frac{\bar{\beta}\bar{\eta}Da_o}{\beta'_o\left[1 + \bar{\eta}Da_o\left(\frac{Bi_m}{Bi_h} - 1\right)\right]}$$

or by Eq. (26), letting $r = Bi_m/Bi_h$,

$$\Delta T_x/\Delta T_o = r\bar{\eta}Da_o/[1 + \bar{\eta}Da_o(r - 1)] \qquad (28)$$

Typical results, expressed as percent of ΔT_o residing in the external film are set forth in Fig. 11 for a range of mass to thermal Biot number ratios, r. Note that for any value of r, as $\bar{\eta}Da_o \to 1.0$, $\Delta T_x/\Delta T_o \to 100\%$.

Practical Implications

Two characteristics of monolith catalyst behavior challenge the analyst:

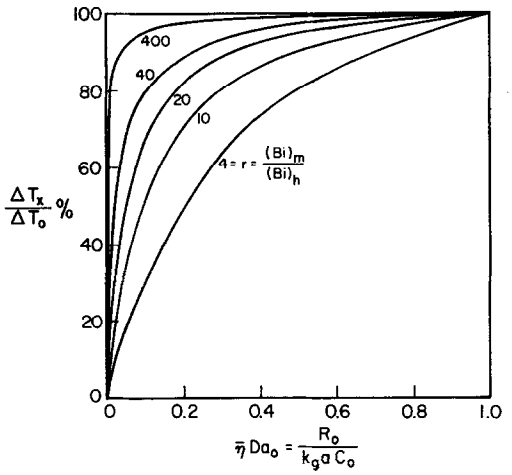

Fig. 11. % of total intra-interphase temperature difference which resides in the external boundary layers as a function of the observable.

1. A phenomenally high rate of global reaction, and not unrelated thereto,

2. "Burn-out" behavior of such magnitude that the monolith mass is occasionally actually disintegrated.

The high rate of activity simply suggests a large if not total contribution of external mass transport to global reaction. In point of fact said mass transport influence, as revealed by the value of $\bar{\eta}Da_o$, is rather neatly anticipated in the analytical and graphical revelations set forth in this paper [Eqs. (11) and (15) and Figs. 2, 3, and 8]. Note particularly that in the case of negative order ($n = -1$) global effectiveness can assume rather large values, since at $n = -1$

$$\bar{\eta} = \frac{1}{(1 - \bar{\eta}Da_o)} \exp\left[-\epsilon_o\left(\frac{1}{t} - 1\right)\right] \qquad (29)$$

This instance is not an idle one, for the oxidation of CO by oxygen over Pd, Pt, Rh, and Ru (*16*) obeys the rate law (in excess oxygen)

$$\mathfrak{R} = k/\mathrm{CO}$$

at concentrations of CO above perhaps 0.5% CO. Thus Fig. 6 applies for the unlikely isothermal circumstance ($\bar{\eta} \geqq 1.0$) and Figs. 2–3, and Eq. (11) apply for the rather likely condition of nonisothermality ($\bar{\eta} \gg 1.0$). This negative order case thus yields effectiveness factors far in excess of unity with consequent excessive heat generation per unit volume of catalyst mass. This fact leads to the second characteristic, "burn-out," or excessive heat generation per unit volume which is surely an explicable phenomena in view of negative-order kinetics. In fact, even if positive order prevails (which is indeed the case for Pd, Pt, Rh, and Ru, at % CO $< 0.5\%$), $\bar{\eta}$ values greater than unity prevail (Figs. 4 and 5).

Hence the observed high rate of reactor activity and "burn-out" are both rationalized by the model presented here.

Some insights into the general problem are to be secured by an inspection of the gas and solid temperatures to be expected in the monolith catalytic oxidation system.

Given the reactivity-heat release character per unit volume, the assumption of adiabaticity is not unreal. Under such circumstances, gas temperature at any point relative to feed temperature T_f is

$$T_o/T_f = \tau = 1 + \beta_f x, \qquad (30)$$

where

$$\beta_f = [(-\Delta H)/\rho C_p T_f]C_f \qquad (31)$$

while solid surface temperature relative to feed temperature is

$$T_s/T_f = \tau + \bar{\beta}_f(1 - x)\bar{\eta}Da_o. \qquad (32)$$

For any surface kinetic situation under conditions of total bulk mass transport control; $\bar{\eta}Da_o \to 1.0$, but by Eqs. (30) and (32)

$$t_x = 1 + \beta_f x + \bar{\beta}_f(1 - x).$$

Since $\bar{\beta}_f = \beta_f \cdot \frac{1}{Le^{2/3}}$, then at $\bar{\eta}Da_o = 1.0$,

$$t_x = 1 + \beta_f[x - (1/Le^{2/3})(x - 1)] \to (1 + \beta_f) \text{ at } Le^{2/3} = 1$$

so that the catalyst surface temperature is constant at the adiabatic reaction temperature when $Le^{2/3}$ is unity. It is small wonder that "burn-out" occurs, given even modest values of β_f for CO and hydrocarbon oxidation. In any event, we should recall that the Lewis number (ratio of Schmidt to Prandtl numbers) can be equal to, less than or greater than unity, hence if $Le^{2/3}$ is less than unity, surface temperatures greater than the adiabatic temperature will result with a rather handsome likelihood of monolith melting.

Indeed in the instance of CO oxidation, as found by Tajbl and Mitani (*16*), the values of ϵ_o to be expected are in the range of 20–30, while $\bar{\beta}$ is in the range of 0.5–1.0, depending, of course, on prevailing concentrations and temperatures. These findings, coupled with observations of negative order in CO, indicate the relevance of results set forth above. Enthalpy changes in the case of hydrocarbon, olefin and aromatic oxidation are even greater than that of CO oxidation; hence $\bar{\beta}$ will indeed be large with respect to total oxidation of these known components in engine exhaust streams.

Stability in CO Oxidation

As we have noted above, CO oxidation over Pt, Pd, etc. is kinetically characterized by negative first order behavior in CO, at conversion levels approaching 100%. We believe (*16*) that, in general, the kinetic model is of the form

$$\mathcal{R} = k(\mathrm{CO})(\mathrm{O_2})/(1 + \mathrm{KCO})^2 \qquad (33)$$

so that for large values of K and conversions of CO less than 100%

$$\mathcal{R} = k\mathrm{O_2}/\mathrm{CO} \qquad (34)$$

while at conversions approaching 100%,

$$\mathcal{R} = k(\mathrm{O_2})(\mathrm{CO}). \qquad (35)$$

So it is that the rate increases with conversion when Eq. (34) applies (abnormal kinetics) while normal kinetics finally dominate [Eq. (35)] at very low CO concentrations, or high conversion. In general [Eq. (33)] one can expect even under isothermal conditions, two steady states and one, intermediate, unstable condition in the gas–solid mass transport–reaction balance at a point. For example, equating bulk mass transport to reaction of negative order [Eq. (34)], and solving for conversion, we find in excess oxygen,

$$x = [1 \pm (1 - 4Da)^{1/2}]/2 \qquad (36)$$

which yields two positive solutions for $Da < 0.25$, where for $n = -1$,

$$Da = kC_o^{-2}/k_g a.$$

When positive linear kinetics prevail ($n = 1$), Eq. (35), but one solution of the local mass transport–surface reaction balance exists. Therefore, over the range of total CO conversion upon Pt, Pd, etc., two stable and one unstable isothermal situations are manifest.

Bearing that in mind, it is clear that when we explore thermal stability, i.e., the heat generation–removal balance in the instance of negative order reaction we can encounter five solutions, two of which are unstable.

Furthermore, in the instance of negative-order kinetics, backmixing or axial dispersion of mass magnifies reactivity; a re-

sult quite contrary to that found with normal (positive order) kinetics. This fact coupled with thermal backmixing which surely enhances reactivity and the unique stability problems cited above, focuses attention upon plausible causes of instabilities observed with noble metal catalysts, particularly on monoliths where radial heat transfer is not as effective as may be expected in a packed bed of pellets.

Summary

The local non-isothermal catalytic effectiveness factor for any reaction order, n, in the case of catalysis upon a nonporous monolith is concisely given by

$$\bar{\eta} = (1 - \bar{\eta}Da_o)^n \times \exp\left[\epsilon_o\left(\frac{1}{1 + \bar{\beta}\bar{\eta}Da_o} - 1\right)\right], \quad (11)$$

where $\bar{\eta}Da_o$ is the ratio of the observed global rate to that of a computable bulk mass transport rate.

Should the monolith substrate be porous, effectiveness for linear kinetics is also given in analytical form:

$$\bar{\eta} = \frac{\tanh \phi}{\phi\left[1 + \frac{\phi \tanh \phi}{(Bi)_m}\right]} \exp\left[-\epsilon_o\left(\frac{1}{t} - 1\right)\right] \quad (15)$$

where for a given value of ϕ, the observable is

$$\bar{\eta}Da_o = \frac{\phi \tanh \phi}{(Bi)_m\left[1 + \frac{\phi \tanh \phi}{(Bi)_m}\right]}, \quad (18)$$

which provides the $\bar{\eta}Da_o$–ϕ relation and, therefore, the isothermal porous substrate effectiveness relationship for external heat and mass gradients.

In the case involving internal–external concentration–temperature gradients, the % of the overall temperature difference which resides in the external boundary layers is

$$\Delta T_x/\Delta T_o = r\bar{\eta}Da_o/[1 + \bar{\eta}Da_o(r - 1)], \quad (28)$$

where $r = (Bi)_m/(Bi)_h$.

Monolith catalyst surface temperature at total mass transport control is given by

$$T_s/T_f = t_x = 1 + \beta_f[x - (1/Le^{2/3})(x - 1)]$$

In view of Eq. (28) and Fig. 11, and the large values of r which characterize gas–porous catalyst systems, Eq. (15) can be applied not only to the monolith system but to exhaust abatement catalysts in the form of pellets.

Finally, consideration of both isothermal and thermal stability for negative order kinetics as found in CO oxidation as catalyzed by noble metals, suggests the existence of multiple stable and unstable states which can surely account for the observed behavior of catalytic fume abatement systems.

Nomenclature

a	surface to volume ratio, cm^{-1}
$(Bi)_h$	thermal Biot number, hL/λ
$(Bi)_m$	mass Biot number, $k_gL/\mathfrak{D}$
C_s	surface concentration, moles/cm^3
C_m	catalyst centerline concentration
C_o	bulk fluid concentration, moles/cm^3
C_p	heat capacity, cal/gm°C
D	molecular diffusivity, cm^2/sec
$\mathfrak{D}$	intraparticle diffusivity, cm^2/sec
Da_o	Damköhler number, equation 4
exp	exponential
E	activational energy
h	interphase heat transfer coefficient, cal/cm^2 sec °C
$-\Delta H$	reaction enthalpy change
j_D	mass transfer j factor, $(k_g/u)(Sc)^{2/3}$
j_H	heat transfer j factor, $(h/\rho uC_p)(Pr)^{2/3}$
k_s	chemical rate coefficient at surface T_s
k_o	chemical rate coefficient at bulk T_o
k_g	interphase mass transfer coefficient, cm/sec
L	volume to surface ratio, cm, $1/a$
Le	Lewis number, Sc/Pr, Eq. (9)
n	reaction order
Pr	Prandtl number, ν/α
r	Biot number ratio, $(Bi)_m/(Bi)_h$
$\mathcal{R}_o$	observed reaction rate, moles/$cm^3 \cdot$ sec $\equiv R_3$ in Figures
R	gas constant
Sc	Schmidt number, ν/D

t	reduced temperature, T_s/T_o
T_m	catalyst centerline temperature
T_o	bulk temperature, °C
T_s	surface temperature, °C
tanh	hyperbolic tangent
u	fluid velocity, cm/sec
x	conversion
z	distance, cm
$\bar{\beta}$	interphase adiabatic $\Delta T/T_o$; $(-\Delta H)C_o/\rho C_p T_o Le^{2/3}$
β_f	overall adiabatic $\Delta T/T_o$; $(-\Delta H)C_f/\rho C_p T_f$
β'	Prater number, $(-\Delta H)C_s\mathfrak{D}/\lambda T_s$ at surface C and T
β'_o	Prater number, $(-\Delta H)C_o\mathfrak{D}/\lambda T_o$ at bulk C and T
ϵ_o	Arrhenius number, E/RT_o
$\bar{\eta}$	ratio of rate at surface conditions, C_s, T_s to that at bulk conditions, C_o, T_o
ϕ	Thiele Modulus

References

1. Wheeler, A., *in* "Catalysis" (P. H. Emmett, Ed.) vol. 2, Reinhold, New York 1955.
2. Weisz, P. E., Swegler, E. W., *J. Phys. Chem.* **59**, 823 (1955).
3. Carberry, J. J., *Chem. Eng. Sci.* **17**, 675 (1962).
4. Thiele, E. W., *Ind. Eng. Chem.* **31**, 916 (1939).
5. Carberry, J. J., *AIChE J.* **7**, 350 (1961).
6. Weisz, P. B., and Hicks, J., *Chem. Eng. Sci.* **17**, 265 (1962).
7. Carberry, J. J., *AIChE J.* **6**, 460 (1960).
8. Aris, R., personal communication (1972).
9. Cassiere, G., and Carberry, J. J., *Chem. Eng. Education, Winter Issue*, **7**, 22 (1973).
10. Hutchings, J., and Carberry, J. J., *AIChE J.* **12**, 30 (1966).
11. Carberry, J. J., *Ind. Eng. Chem.* **58**(10) 40 (1966).
12. Goldstein, W., and Carberry, J. J., *J. Catal.* **28**, 33 (1973).
13. Prater, C. D., *Chem. Eng. Sci.* **8**, 284 (1958).
14. Mercer, M. C., and Aris, R., *Lat. Amer. J. Chem. Eng. Appl. Chem.* **2**, 149 (1971).
15. Lee, J. C. M., and Luss, D., *Ind. Eng. Chem. (Fund)* **8**, 596 (1969).
16. Tajbl, D. G., Simons, J., and Carberry, J. J., *Ind. Eng. Chem. (Fund)* **5**, 171 (1966). See also Tajbl, D. G., Ph.D. Thesis, Univ. of Notre Dame (1966) and Mitani, T., MS Thesis, Univ. of Notre Dame (1969).